Protected superconductivity at the boundaries of charge-density-wave domains

Brigitte C. Leridon, Sergio Caprara, Johan Vanacken, V. V. Moshchalkov, Baptiste Vignolle, Rajni Porwal, R. C. Budhani, Alessandro Attanasi, Marco Grilli, José Lorenzana

PAPER • OPEN ACCESS

Protected superconductivity at the boundaries of charge-density-wave domains

New Journal of Physics
The open access journal at the forefront of physics

Deutsche Physikalische Gesellschaft DPG
IOP Institute of Physics

Published in partnership with: Deutsche Physikalische Gesellschaft and the Institute of Physics

OPEN ACCESS

RECEIVED
9 January 2020

REVISED
23 April 2020

ACCEPTED FOR PUBLICATION
28 May 2020

PUBLISHED
20 July 2020

PAPER

Protected superconductivity at the boundaries of charge-density-wave domains

Brigitte Leridon[1,6], Sergio Caprara[2], J Vanacken[3], V V Moshchalkov[3], Baptiste Vignolle[4,7], Rajni Porwal[5], R C Budhani[5,8], Alessandro Attanasi[2], Marco Grilli[2] and José Lorenzana[2,6]

[1] LPEM, ESPCI Paris, CNRS, Université PSL, Sorbonne Universités, 10 rue Vauquelin, 75005 Paris, France
[2] ISC-CNR and Department of Physics, Sapienza University of Rome, Piazzale Aldo Moro 2, I-00185, Rome, Italy
[3] KU Leuven, Celestijnenlaan 200 D, B-3001 Leuven, Belgium
[4] LNCMI (CNRS, EMFL, INSA, UJF, UPS), Toulouse 31400, France
[5] CSIR-National Physical Laboratory, New Delhi-110012, India
[6] Author to whom any correspondence should be addressed.
[7] Present address: CNRS, Univ. Bordeaux, ICMCB, UMR5026, F-33600 Pessac, France.
[8] Present address: Morgan State University, 119 Calloway Hall, 1700E Cold spring lane, Baltimore MD 21251, USA.

E-mail: Brigitte.Leridon@espci.psl.eu and jose.lorenzana@cnr.it

Keywords: high-T_c superconductivity, charge-density-wave, filamentary superconductivity, magnetotransport, disorder

Abstract

Solid ^{4}He may acquire superfluid characteristics due to the frustration of the solid phase at grain boundaries. Here, introducing a negative-U generalized Hubbard model and a coarse-grained semiclassical pseudospin model, we show that an analogous effect occurs in systems with competition among charge-density-waves (CDW) and superconductivity in the presence of disorder, as cuprate or dichalcogenide superconductors. The CDW breaks apart in domains with topologically protected filamentary superconductivity at the interfaces. Our transport measurements, carried out in underdoped $La_{2-x}Sr_xCuO_4$, with the magnetic field acting as a control parameter, are shown to be in excellent agreement with our theoretical prediction. Assuming superconductivity and CDW phases have similar energies, at intermediate temperatures, the magnetic field drives the system from a fluctuating superconductor to a CDW as expected in the clean limit. Lowering the temperature, the expected clean quantum critical point is avoided and a filamentary phase appears, analogous to 'glassy' supersolid phenomena in ^{4}He. The transition line ends at a second quantum critical point at high-fields. Within our scenario, the filamentary superconducting phase is parasitic with CDW and bulk superconducting phases playing the role of primary competing order parameters.

1. Introduction

Electrons in the presence of attractive interactions crossover smoothly from the Bardeen–Cooper–Schrieffer limit to the Bose condensation limit as the strength of the interaction is increased [1]. However, as electrons approach the limit of composite bosons, the tendency to localize in real space also increases. Thus, in analogy with ^{4}He, a real-space ordered state competes with a momentum-space condensed state. Since the entropy of these states is equally small [2], phase stability is insensitive to temperature, resulting in a phase boundary nearly parallel to the T axis and perpendicular to any non-thermal control parameter axis (pressure, strain, magnetic field, doping, etc).

The scenario changes dramatically in the presence of real-space disorder. It has been known for some time that a polycrystal of ^{4}He atoms develops superfluidity at the interface and acquires supersolid characteristics (i.e., superfluid-like changes of the moment of inertia coexisting with real-space order, see reference [3] for a review). It is natural to expect that the analogous phenomenon should occur for real-space fermion pairs [4]. In this work, we consider a simple phenomenological model which allows to study the effect of quenched disorder near a transition from a real-space ordered state of fermion pairs to a superconducting state. We show that disorder induces filamentary superconductivity in the spatially ordered

charge-density-wave (CDW) state analogous to the supersolid behavior in ^{4}He. A finite temperature phase diagram is derived. This theoretical scenario is explored experimentally by transport experiments in $La_{2-x}Sr_xCuO_4$ (LSCO) using magnetic field as a tuning parameter. Building on a previous work [5] we perform a global two-dimensional fitting of all magnetoresistivity data in the (H, T) plane. Setting the doping close to the insulator-superconductor transition enables to completely suppress superconductivity at high field and, by subtraction, isolate the paraconductive contribution. This more accurate study performed for two specific doping values, with a high number of temperature points confirms the general trends found in a wider doping range in reference [5], and enables to demonstrate the excellent qualitative agreement between the experimentally derived transition lines and the theoretical expectations. At moderate temperatures there is a magnetic field driven transition between the superconductor and a charge-ordered state, as seen with other probes [6]. Lowering the temperature in the CDW phase, a superconducting phase appears, characterized by small superconducting stiffness and due to the coherent phase-locking of superconducting filaments at the interfaces of CDW domains, analogously to the supersolid effects in ^{4}He. Filamentary superconductivity in cuprates has been proposed before [7].

2. Theory of disorder-induced filamentary superconductivity on charge-density-waves

2.1. CDW domain wall in the generalized attractive Hubbard model

We consider an electronic system with an attractive interaction that favors real-space formation of fermion pairs. At low temperatures these pairs can either condense in a superconducting state or form a CDW. An instructive example to study this interplay (sometimes referred to as intertwining [8]) is the negative-U generalized Hubbard model in a bipartite lattice,

$$H = -t\sum_{\langle ij\rangle\sigma} c^\dagger_{i\sigma}c_{j\sigma} - U\sum_i n_{i\uparrow}n_{i\downarrow} + V\sum_{\langle ij\rangle\sigma} n_i n_j \tag{1}$$

where $c^\dagger_{i\sigma}$ creates a fermion with spin σ at site i, $n_{i\sigma} = c^\dagger_{i\sigma}c_{i\sigma}$, $n_i = n_{i\uparrow}n_{i\downarrow}$, $U > 0$ is the on-site attraction, V denotes a nearest neighbor repulsion, t denotes the hopping amplitude, and μ is the chemical potential.

The repulsive-attractive transformation [9] allows to map the negative-U Hubbard model into a positive-U Hubbard model using a construction analogous to Anderson pseudospins [10]. The on-site magnetization of the repulsive model $\mathbf{m}_i$ maps into the charge sector of the attractive model as follows,

$$\begin{aligned} m_i^x &= \frac{1}{2}\left(\langle c^\dagger_{i\uparrow}c^\dagger_{i\downarrow} + c_{i\downarrow}c_{i\uparrow}\rangle\right) e^{i\mathbf{Q}\cdot\mathbf{r}_i} \\ m_i^y &= -i\frac{1}{2}\left(\langle c^\dagger_{i\uparrow}c^\dagger_{i\downarrow} - c_{i\downarrow}c_{i\uparrow}\rangle\right) e^{i\mathbf{Q}\cdot\mathbf{r}_i} \\ m_i^z &= \frac{1}{2}\left(\langle c^\dagger_{i\uparrow}c_{i\uparrow} + c^\dagger_{i\downarrow}c_{i\downarrow}\rangle - 1\right). \end{aligned} \tag{2}$$

Thus, at half-filling the CDW (superconducting) order of the attractive model is mapped into antiferromagnetic order along the z axis (in the xy plane). It is convenient to define a staggered order parameter $\mathbf{S}_i = \mathbf{m}_i \exp(-i\mathbf{Q}\cdot\mathbf{r}_i)/|\mathbf{m}|$ with $\mathbf{Q} = (\pi, \pi)$ in two dimensions and in units of the inverse lattice constant and $|\mathbf{m}|$ is taken as the largest on-site magnetization of the lattice.

For $V = 0$ the repulsive model has SO(3) symmetry in the magnetic sector which means that in the attractive model CDW and superconductivity are degenerate. This symmetry is also obvious from the large U limit of the repulsive model which maps in the Heisenberg model with magnetic interaction $J \approx 4t^2/U$. This symmetry is not generic and gets explicitly broken by a nonzero nearest-neighbor interaction. $V < 0$ favors the superconducting state, i.e., an order parameter with xy symmetry. In the opposite case of nearest-neighbor repulsion, an Ising symmetry is favored, corresponding to the CDW [9].

The model supports two variants of the CDW (labeled A and B) differing on which of the two sublattices hosts more charge than the other, which corresponds to the two possible z-antiferromagnetic ground states of the repulsive model. A positive (negative) S_i^z describes the A- (B-) CDW. Figure 1(a) shows the order parameter space. We are interested in situations in which the CDW is more stable but disorder is present favoring A-CDW in one region and B-CDW in a different region. For large U, the only way to reverse the order parameter is by passing through the equator, the interface is forced to have ordering on the xy plane, and is locally superconducting, as shown schematically in figure 1(b).

In order to analyze this effect for general U and V we have solved the model equation (1) in the Hartree–Fock–Bogoliubov–de Gennes approximation in two dimensions. We have taken periodic

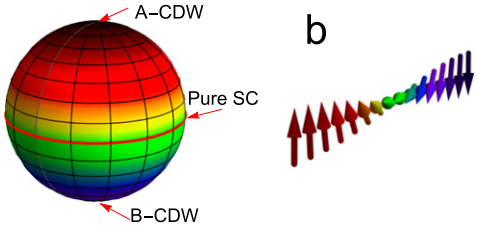

Figure 1. (a) The sphere represents the states encoded by the order parameter with near SO(3) symmetry. North and south poles represent the two possible CDW states, corresponding to the charge maximum in one of the two possible sublattices, while the equator encodes the superconducting state. The azimuthal angle encodes the phase of the order parameter. (b) Schematic pseudospin pattern at an interface between B/A-CDWs.

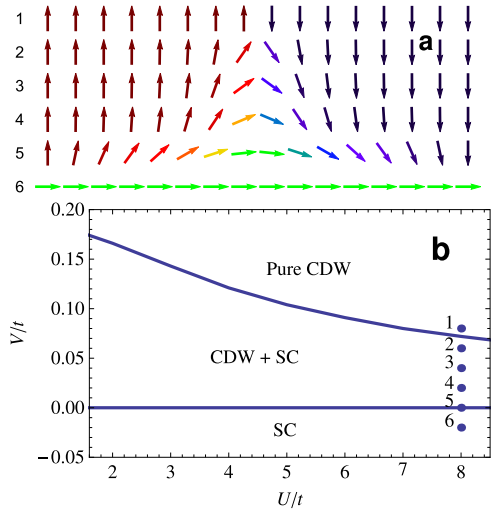

Figure 2. (a), Evolution of a domain wall between the two variants of the CDW as the nearest neighbor repulsion V is decreased from row 1 to row 6. The order parameter $\mathbf{S}_i$ (staggered pseudomagnetization) in the $x-z$ plane is pictured as a function of position perpendicular to the interface (the superconducting phase ϕ is set to zero). We use the same color convention as in figure 1. Only one row is shown for each configuration since there is translational invariance along the interface. The attractive U is fixed at $U/t = 8$ and V is decreased in equal steps from $V = 0.08t$ for row 1, to $V = 0^+$ for row 5. For repulsion comparable to $J \approx 4t^2/U$ (row 1) the interface is sharp and there is no superconducting component. Below a critical repulsion a superconducting component appears (given by the horizontal projection of the arrows) which grows as V is decreased (rows 2–5). Row 6 shows the bulk superconducting phase obtained for negative V. (b), Phase diagram for the interface between the two variants of the CDW as function of the parameters of the electronic model. The parameters for the configurations pictured in figure 2(a) are indicated with dots. There is a second-order-phase-transition line between the superconducting interface (CDW + SC) and the sharp CDW interface. For negative V the bulk ground state is always superconducting (SC). In a finite system, the boundary is at a small positive V due to the cost of the domain wall.

boundary conditions and worked in a system of size $L_x \times L_y = 15 \times 100$ sites. The odd number of sites in the x direction forces a domain wall of the staggered order, which we wish to study.

In figure 2(a) we show the evolution of an interface between the two CDW variants that have been imposed by boundary conditions and in figure 2(b) we show the resulting phase diagram. Below a critical line the interface becomes superconducting. Thus, in the presence of a relatively strong pairing scale, pairs may localize in real space forming a CDW, but the interface between the different variants will be superconducting, provided the system is close enough to the suerconducting phase. Remarkably, this behavior persist and is even enhanced for small values of U. Very small U was not analyzed as the coherence length becomes of the order of our simulation cell and finite size effects become important. Notice that when the order parameter is on the z axis (pure CDW) the superconducting order-parameter phase ϕ is ill defined thus a CDW domain is nothing but a collection of phase incoherent pairs.

2.2. Coarse-grained model

We now turn to a semiclassical model, in order to analyze the effect of interfaces induced by disorder on mesoscopic scales. It is natural to assume that in a region of parameter space in which charge order and superconductivity are seen to coexist, the near SO(3) degeneracy is reestablished and a model with that symmetry generically describes a situation in which the energy for real-space (i.e., CDW) or momentum-space (i.e., superconducting) condensation of paired fermions is comparable. Indeed, a lattice

model very similar to our proposal below has been considered by Liu and Fisher to study possible supersolid phases in ^{4}He [11] close to the boundary between the crystalline phase and the superfluid phase underling the close analogy between ^{4}He and the superconductivity-CDW problem.

Since we are interested in intertwining, and in the finite temperature phase diagram, we will neglect quantum fluctuations. These become important when the temperature is below the characteristic energies of the problem, which, especially in the filamentary superconducting region, are very low. Thus we will study a semiclassical model of superconductivity-CDW, building on the above solution of the negative-U model and in the spirit of reference [11] for the supersolid problem.

A generic semiclassical model can be justified by a coarse-graining process. The order parameter $\boldsymbol{S}_i$ has the same number of components as in the generalized Hubbard model above, so also here figure 1(a) displays the order-parameter space and for simplicity we will use the same symbol. Assuming that there is at least short range order in the system we can separate it in regions larger than the lattice spacing but smaller than the correlation length and define the coarse-grained ordering field $\boldsymbol{S}_i$ which determines the kind of order in region i. We neglect the fluctuations in the strength of fermion pairing which is parameterized by the magnitude of the ordering field so we take $|\boldsymbol{S}_i| = 1$. Thus we assume that the CDW consists of localized bosons which in the context of insulator-superconducting transitions is associated with a Mott–Hubbard bosonic insulating phase [12]. We also neglect all complications due to unconventional symmetry of the order parameter. In addition, we assume that there are only two possible variants of CDW phases as for the Hubbard model so $S^z = 1$ ($S^z = -1$) encodes the A(B)-CDW as for the generalized Hubbard model above. In general, more variants will be possible depending on the periodicity of the CDW. In the discussion section below, we enumerate possible microscopic origins of the different CDW variants. Our considerations are, however, independent of these microscopic details. As before, a pure superconducting state is described by the complex ordering field $S_i^x + \mathrm{i}S_i^y$ with $S^z = 0$, while sideways configurations describe the CDW analog of supersolid behavior as in reference [11]. We define the semiclassical model on a discrete lattice of cells which is convenient for numerical simulations,

$$H = -J\sum_{\langle i,j\rangle} \boldsymbol{S}_i \cdot \boldsymbol{S}_j - G\sum_i (S_i^z)^2 + \sum_i h_i S_i^z. \tag{3}$$

Here, $J > 0$ describes a short-range stiffness which, for simplicity, we choose to be equivalent for superconducting correlations and CDW correlations. In the absence of disorder ($h_i = 0$), the balance between the orders is decided by the parameter G which plays the same role as V in the generalized Hubbard model. Thus, $G > 0$ describes a uniform CDW while $G < 0$ describes a uniform superconductor. One could as well have used an anisotropic Heisenberg model with the same scope which, at the classical level we are considering, would only change minor details. h_i is a random variable that takes into account that charged impurities will locally favour the A- or B-CDW, depending on whether the impurities in the cell i have more charge near the A or the B sublattice. We will take the h_i to be random variables with a flat probability distribution between $-W$ and W and, since we are interested in layered systems (cuprates, dichalcogenides), we will consider a two-dimensional system.

For $G > 0$ the model falls into the universality class of the random-field Ising model. As such, for any disorder, it breaks apart in domains of the A- and B-CDW variants. This is obvious for large disorder while for small disorder it follows from Binder's refinement [13] of Imry's and Ma's arguments [14]. In the latter case, however, domains can be exponentially large [roughly $\propto \exp(J^2/W^2)$].

For $G > 0$ one can consider a flat interface between an A-CDW and a B-CDW. As for the generalized Hubbard model in figure 2 the interface is forced to have the ordering field on the xy plane. In the present model, by minimizing the energy, one finds that the superconducting region has width $\xi_g = \xi_0\sqrt{J/G}$ where ξ_0 is a short-range cutoff of the order of the coarse-grained lattice spacing corresponding to the correlation length of the short-range superconducting (i.e., particle-particle) or CDW (i.e., particle-hole) pairs. Thus, although for $G > 0$ the superconductor is globally less stable, it gets stabilized locally because of topological constraints as for the CDW interface in figure 2. In the interface both CDW are frustrated so the less stable superconducting phase prevails as in polycrystalline ^{4}He.

It is convenient to write the model in spherical coordinates with $S_i^z = \sin\ \theta_i$ and $S_i^x + \mathrm{i}S_i^y = \cos\ \theta_i \exp(\mathrm{i}\phi_i)$. Clearly, $\cos\theta_i$ and ϕ_i are the amplitude and phase of the superconducting order. Equation (3) reads,

$$H = -J\sum_{\langle i,j\rangle} \cos\ \theta_i\ \cos\ \theta_j\ \cos(\phi_i - \phi_j) - G\sum_i \sin^2\ \theta_i + \sum_i h_i\ \sin\ \theta_i. \tag{4}$$

To analyze the interplay between superconductivity, CDW and disorder, the energy of the model was minimized using a steepest descent algorithm. Figure 3 shows configurations obtained by minimizing the functional equation (4) at $T = 0$, with different disorder strengths. Blue and red corresponds to the A- and

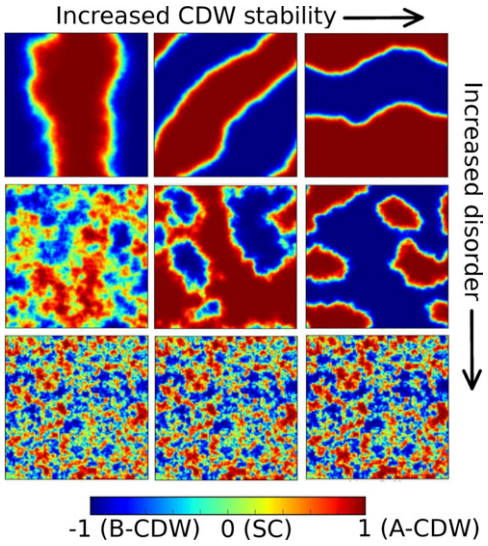

Figure 3. Zero temperature configurations obtained by minimizing the energy functional equation (3). The control parameter is taken to be $G > 0$, so in the absence of disorder the system is in the CDW phase. The size of the system is 100×100. The false color plots represent S_z; blue and red regions correspond to the two CDWs and light green regions are the superconducting regions. For every row, the control parameter G increases from left to right $G/J = 0.02, 0.06, 0.1$. For every column, disorder increases from top to bottom with the following strength: $W/J = 0.5, 1.5, 4.0$.

B-CDW respectively. For small $G > 0$ and small disorder (upper left corner), large domains are present. As for the flat interface, the pseudospin at the boundary of the two CDW domains is in the xy plane. In other words, it forms a filament of superconducting order (light green). If disorder is changed locally, for example the random fields are flipped one-by-one, then the filament moves without being annihilated, a hallmark of topological protection. Only a global disorder change that eliminates a whole CDW domain is able to eliminate the associated superconducting filament. We associate the network of filaments with filamentary superconductivity. Such network becomes denser when increasing disorder (from top to bottom in the figure). We anticipate that this effect can lead to an increasing superconducting stiffness.

The superconducting phase is uniform along the filamentary superconducting regions so that at $T = 0$, if the interfaces form a percolative path, the system is globally superconducting. From left to right, the local CDW stability (controlled by G) increases. Filamentary superconducting regions become narrower as $\xi_g \propto 1/\sqrt{G}$, increasing the CDW tendency. This will of course tend to weaken the superconducting stiffness as discussed below.

We define the global superfluid stiffness from the second derivative of the energy respect to a twist of the boundary conditions $\rho_s \equiv \partial^2\langle H\rangle/\partial\Delta\phi^2$ where $\Delta\phi$ is the difference in phase ϕ_i between opposite sides of the system in one direction. To compute ρ_s we mapped the problem into a random resistor network where nodes i, j are connected with a conductance of magnitude $g_{ij} = J\cos\theta_i\cos\theta_j$. Notice that g_{ij} acts as a local xy superfluid stiffness in equation (4). The macroscopic ρ_s is mapped into the global conductance of the network which we find in the linear response regime by solving numerically the equivalent network problem [4, 15]. Result for each parameter were averaged over 200 different configurations.

For zero disorder (light green in figure 4) the stiffness jumps from the bare value to zero as the systems changes abruptly from the superconducting to the CDW state at $G^* = 0$. Inside the superconducting region ($G < G^*$) disorder induces non-zero θ_i as charges get localized, so that g_{ij} gets weakened and the global stiffness is reduced. However, entering into the CDW region ($G > G^*$) the stiffness develops a 'foot' for positive G indicating that filamentary superconductivity is induced in the nominally CDW region (blue and magenta in figure 4). For large detuning from $G^* = 0$ phase stiffness is suppressed exponentially, roughly as $\rho_s \propto \exp[-C(G/J)^3]$, with C a constant depending on the disorder strength (see inset in figure 4). This indicates that an ever more fragile superconducting regime sets in as the tendency to CDW is increased and the filaments forming the network become narrower. We anticipate that the decreasing but finite stiffness will produce a characteristic 'foot' in the temperature dependent phase diagram, which we take as the fingerprint of filamentary superconductivity.

Moderately stronger disorder makes the superfluid phase more robust because the network of filaments becomes denser. At some point, however, for very strong disorder, charge localization is favored at every site and the system becomes an insulating charge glass. The different regimes can be seen by plotting isolines of the phase stiffness as shown in figure 4(b). We see that, with increasing disorder, filamentary

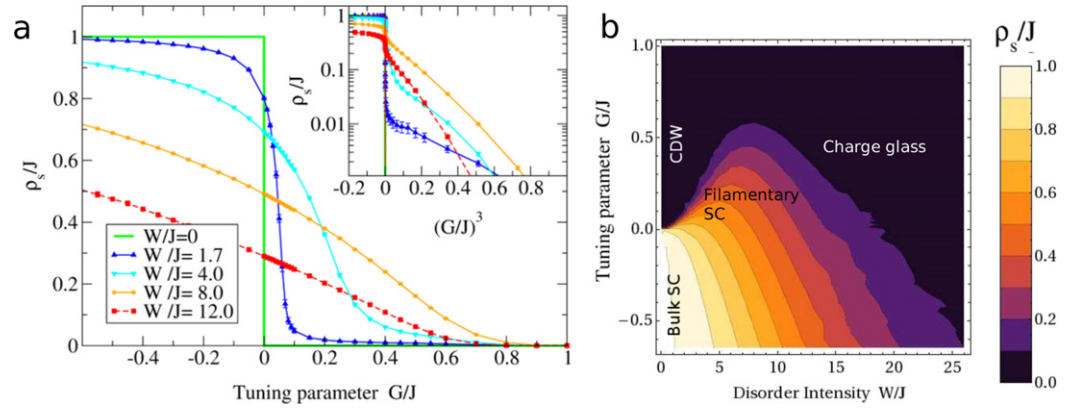

Figure 4. (a) Zero temperature stiffness as a function of the tuning parameter G/J for different strengths of disorder and system size 100×100 sites as in figure 3. The inset shows the same quantity in semi-log scale as a function of $(G/J)^3$. (b) False color plot of the stiffness as a function of tuning parameter and disorder.

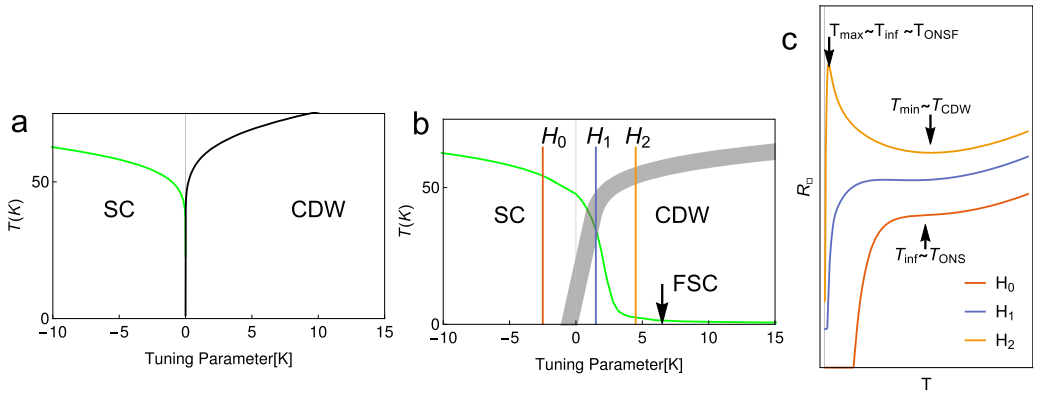

Figure 5. Schematic phase diagram in the clean limit (a) and with small disorder (b). The sharp transition line to the CDW phase in the clean case (black full line) becomes a crossover in the disordered case (gray band). To establish a qualitative connection with transport experiments in LSCO we schematically indicate the role of magnetic field as the tuning parameter. In panel (c) we then report the expected behavior of the resistivity in the different regions of the (dirty) phase diagram. Curves have been shifted vertically for clarity. For $H = H_0$, the resistivity is expected to be a decreasing function of temperature. For $H = H_1$ and high temperatures the resistivity will exhibit a plateau due to the residual influence of the clean quantum-critical point. Lowering the temperature, disorder becomes relevant and eventually the system becomes superconducting. For $H = H_2$, the resistivity will exhibit a minimum when the CDW correlations set in and a maximum before dropping due to the filamentary superconducting phase. The arrows indicate the characteristic temperatures discussed in the text.

superconductivity is a reentrant phase in the CDW region. Interestingly, for a fixed control parameter $G > 0$, there is an optimum value for disorder to induce superconductivity.

Although this phase diagram is for zero temperature, we can derive a finite temperature phase diagram assuming that in the clean limit the system behaves as an anisotropic Heisenberg model [16] (figure 5(a)) and in the presence of disorder develops a finite temperature superconducting phase with a T_c proportional to the *xy* phase stiffness [17]. Figure 5(b) shows schematically the modified phase diagram in the presence of small disorder. Here, we have assumed that T_c is proportional to the stiffness of the $W/J = 1.7$ case in the filamentary region. For negative tuning parameter, T_c interpolates smoothly to the T_c of the clean limit, so as the stiffness does (figure 4(a)). We have chosen the microscopic parameters so that the energy scale represents typical values of underdoped cuprates. In the filamentary superconducting phase the CDW domains coexists with superconductivity (figure 3). The CDW transition gets broadened by the effect of disorder, so that the sharp Ising-like transition of the clean case becomes a crossover (gray band) with glassy characteristics in the presence of disorder [18]. In the case of unidirectional CDW a sharp transition may persist in a nematic channel, as discussed in references [19, 20].

In order to associate the phase diagram to magnetotransport experiments, we will define below characteristic temperatures from resistivity data and assume they can be used as proxies of the different transition or crossover lines. A guide to the various temperature scales introduced in this work can be found in table 1.

Table 1. Guide to the meaning of the various temperature scales introduced in the text. The horizontal line separates temperature scales that are introduced in the theory and/or the fitting formulas from temperature scales that are defined by the experimental temperature dependence of the measured resistance $R_{\square}(T)$.

Temp. scale	Proxy	Meaning
T_c^B	T_c	T_c for bulk superconductivity (SC)
T_c^F	T_c	T_c for filamentary SC (FSC)
T_{ONS}	T_{inf}	Onset of superconducting correlations
T_{ONSF}	T_{inf}	Onset of FSC
T_{CDW}	T_{min}	CDW crossover temperature
T_0	Fit	Cutoff T above which an exponential suppression of paraconductivity occurs
T_1	Fit	Temperature width of low-T suppression of resistance due to FSC
T_c		T at which $R_{\square}(T) = 0$
T_{max}		T at which $R_{\square}(T)$ has a local maximum
T_{min}		T at which $R_{\square}(T)$ has a local minimum
T_{inf}		T at which $R_{\square}(T)$ has an inflection point

Since magnetic field H is known to tip the balance between superconductivity and CDW [6], we will use $H - H^*$ as the tuning parameter where H^* corresponds to the field of a clean quantum-critical point, i.e., zero tuning parameter ($G^* = 0$). Thus, in figure 4(a) we associate the abscissa axis with the magnetic field (increasing from left to right). In the figure, the temperature units of the tuning parameter were approximately derived from equivalent energy units in the microscopic Heisenberg model. Conversion to magnetic-field units would require a precise mapping of the models which is beyond our scope. Empirically, we find that, as an order of magnitude, 5 K of the microscopic model corresponds to 10 T of the experiment.

At zero or low field (H_0, red line in figure 5(b)) the metallic phase directly becomes superconducting, so transport experiments are expected to yield a monotonic decreasing function of temperature, as shown with the red curve in panel (c). We will use the inflection point in this curve T_{inf} (indicated by the arrow in panel (c)) as a function of field as a proxy for T_{ONS}, the characteristic temperature below which robust in-plane superconducting correlations appear. Notice that three-dimensional zero-resistance superconductivity sets in at a lower temperature, T_c. T_{inf} should not be confused with another inflection point appearing around 270 K at this doping and unrelated to superconductivity [21, 22]. At intermediate fields, $H = H_1$, and at high/intermediate temperatures, when disorder is not yet relevant, the system critically fluctuates between the superconducting and CDW states, giving rise to a flat resistance that would seemingly extrapolate to a zero-temperature clean quantum-critical point (located nearly zero tuning parameter). Eventually, however, the clean quantum-critical point is avoided and superconductivity prevails at low T and the resistance vanishes (blue lines). At higher fields ($H = H_2$, orange lines) the metal first enters a region of disordered (polycrystalline) CDW with an insulating behavior, thus the temperature corresponding to the resistivity minimum serves as a proxy of the CDW crossover temperature T_{CDW}, as shown in panel (c). Lowering even more the temperature the resistivity shows an inflection point very close to a sharp maximum, followed by a rapid drop when coherence establishes between the superconducting filaments. We will use the inflection point (near the maximum) to signal the onset of filamentary superconductivity, T_{ONSF}, as shown with the arrow in the upper left corner of panel (c). For weak disorder, the intermediate region showing clean quantum-critical behavior (i.e., the resistivity plateau) is around the region in parameter space where T_{max}, T_{min}, and T_{inf} merge.

3. Filamentary superconductivity in LSCO as revealed by magneto-transport

We expect the scenario presented in the previous section to be realized in underdoped cuprates, where superconductivity and CDW are known to compete. In particular, when a strong magnetic field [6] or strain [23] are present, a static charge order is well documented in the underdoped region of the phase diagram, below a temperature T_{CDW} [24, 25]. This charge-ordered phase breaks apart in domains due to quenched disorder [26] and is believed to be responsible for the Fermi surface reconstruction at doping values below $p = 0.16$ [27–30]. We thus chose to study the resistivity of LSCO thin films with Sr doping slightly above the minimal doping for superconductivity in order to be able to drive gradually the system towards the insulating state by increasing the magnetic field. Two samples with different Sr content were studied in this work, namely $x = 0.08$ (sample 008) and $x = 0.09$ (sample 009).

The thin film for sample 008 was deposited onto $SrTiO_3$ (STO) substrates at KU Leuven, using dc magnetron sputtering as described in reference [33]. For this sample, the resistance as function of magnetic field for different temperatures was measured in KU Leuven high pulsed magnetic field facilities, using four

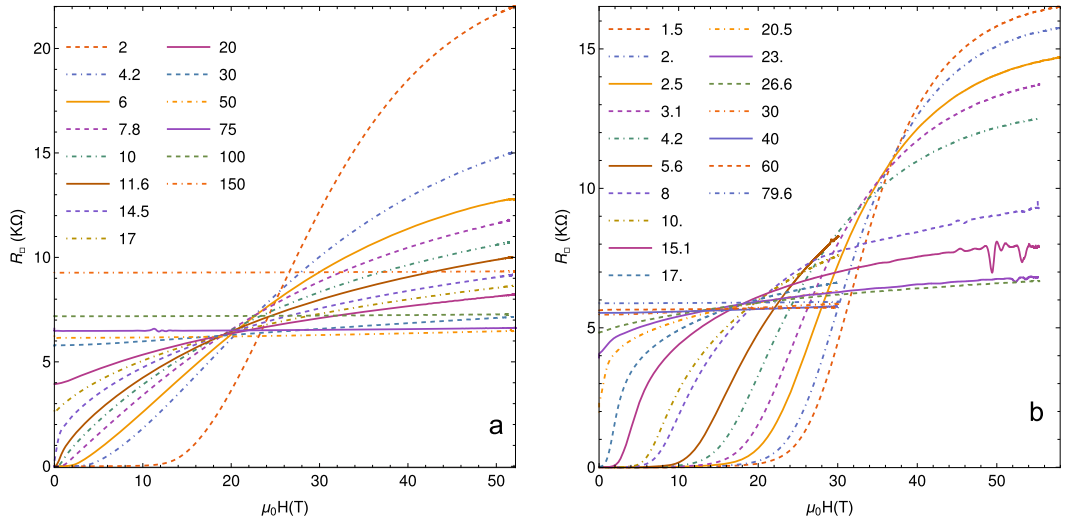

Figure 6. (a) Resistivity versus magnetic field for sample LSCO 0.08 for a given set of temperatures ranging from 2 K to 150 K. (See text for the experimental details.) An accumulation point is clearly visible around 19 T corresponding to the signature of the clean QCP at intermediate temperatures. (b) Resistivity versus magnetic field for sample LSCO 0.09 for a given set of temperatures ranging from 1.5 K to 79.6 K. (See text for the experimental details.) Note that some of the pulses were only performed up to 30 T. Two accumulation points are visible corresponding to the clean QCP (≈18 T) and the high-field QCP (≈36 T). Curves are labeled by the temperature in Kelvin units.

probe measurements on an epitaxial film of thickness $t = 100$ nm, patterned in strips of 1 mm $\times 100\,\mu$m. High-field pulses up to 49 T were applied from 1.5 to 300 K perpendicularly to the *ab*-plane of the *c*-axis oriented films. While applying a nominal ac current of intensity typically about 100 μA at 50 kHz, the voltage across the sample was measured and stored in a transient recorder operating at 1 MHz. In order to avoid any possible artifact due to the superconducting transition during the magnetic field pulse that may affect the current through the sample, the latter was also measured during the pulse. The nominal current density was more than two orders of magnitude below the critical current at low temperature, and it was checked that lowering the current to 10 μA did not affect significantly the measured resistance. In order to remove $\mu_0\,\mathrm{d}H/\mathrm{d}t$ corrections a standard procedure was applied. We performed two successive pulses at each temperature for two opposite directions of the magnetic field and averaged out the measured voltages, that were then amplified and mixed up with a contribution of a $\mu_0\,\mathrm{d}H/\mathrm{d}t$ generated at a pick-up coil of a few turns situated near the sample. This procedure enabled to separate the sweep-rate induced signals in the wiring from the meaningful physical signal. We therefore obtained a set of $R_\square(H, T)$ data.

The 009 thin film was grown by pulsed laser deposition in IIT Kanpur on $LaSrAlO_4$ (LSAO) substrate. This film of typical dimensions 4×4 mm^2 and of thickness $t = 200$ nm was measured in a Van der Pauw geometry. $R_\square(H, T)$ data as a function of field up to 54 T and temperature from 1.5 to 300 K was obtained at LNCMI Toulouse high field facility using similar techniques and procedures, with a typical nominal current intensity of about 10 μA. The experimental resistance versus magnetic field curves are pictured in figure 6. The resistances measured during the increasing and decreasing part of the pulses are very close (only the increasing branch is shown). Although this indicates that the heating effect of the pulse on the measurements is shown to be extremely limited, only the increasing field values were used.

Our goal here is to derive a magnetotransport phase diagram to be compared with the theoretical results. A microscopic computation of transport would be a formidable task as it would require to take into account the quantum nature of quasiparticles, their scattering in the CDW regions, their role in mediating phase coherence between the superconducting filaments, etc [12, 31–34]. Therefore, we avoid in our approach a microscopic attempt to describe the resistivity experiments and we concentrate on the characteristic temperatures which can be extracted from the transport data. Specifically, we assume the crossover lines are well represented by the proxies introduced in the previous section, so we directly extract the phase diagram from the behavior of characteristic temperatures as a function of magnetic field. To find the first and second temperature derivative of the resistivity it is convenient to fit the data as done in reference [5]. Thanks to the fact that we are at a doping very close to the insulator superconducting transition it is possible to completely suppress superconductivity with the highest fields. This allows for a much simpler fit as will be shown below. Indeed, rather than fitting each $R(H, T)$ curve for each H with independent parameters we manage to fit the entire surface in the (H, T) plane at once, with a considerable

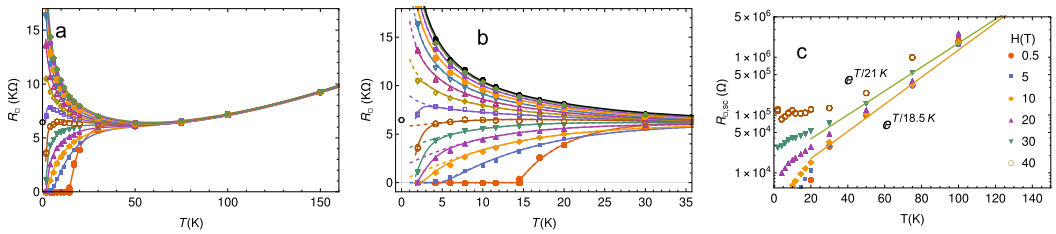

Figure 7. Temperature dependent resistivity for sample 008 (LSCO/STO, $x = 0.08$) for different fields. Panel (a) shows data at selected fields together with the two-dimensional fits. Fields start from $\mu_0 H = 0$ T (hereafter, μ_0 is the magnetic permeability of free space) in the lower curve, up to 48 T, in intervals of 4 T. Panel (b) shows detailed data at low temperatures. The black curve is the fit of the data without superconducting component at 50 T (black dots). Dashed lines are the same fits but without the tanh low temperature cutoff (see text). In (a) and (b), the open black circle at $T = 0$ indicates the quantum of resistance, $R_Q = h/(2e)^2$. Panel (c) is the superconductivity-related resistance in semi-log scale showing the exponential behavior of the resistivity above a cutoff temperature T_0, as shown by the lines.

decrease in the number of fitting parameters. The accuracy of this procedure entails a much more robust method to extract relevant characteristic temperatures, with respect to reference [5].

The fits were obtained considering two independent contributions to the conductivity,

$$[R_\square(H,T)]^{-1} = \left[R_{\square,\mathrm{SC}}(H,T)\right]^{-1} + \left[R_{\square,\mathrm{CO}}(T)\right]^{-1}. \tag{5}$$

The second term on the rhs represents the field independent conductivity in the absence of any superconducting fluctuation and is characterised by a crossover from the linear high-temperature behaviour of resistivity of the metallic state to the logarithmic insulating-like behaviour taking place at low T under strong magnetic fields, that we associate to the formation of the polycrystalline CDW state (charge-ordered state). We therefore assume that this is the high-field behaviour of the system and estimate it by a fit to the higher field data (typically $\mu_0 H = 50$ T) and maintained if fixed for all the fields measured in that sample. For $R_{\square,\mathrm{CO}}(T)$ we used a linear term plus a polynomial in (log T) up to (log T)^3 depending on sample. The resulting $R_{\square,\mathrm{CO}}(T)$ is shown with a black line in figure 7(b) where the data of figure 6(a) is presented for fixed selected H values as a function of temperature. Subtracting this contribution to the total conductivity allows to identify the contribution of superconductivity (static as well as fluctuating) to transport, as represented by the first term in the rhs of equation (5), which also encodes all the significant magnetic field dependence of transport.

The superconductivity-related resistance, $R_{\square,\mathrm{SC}}$, shows that at high-temperature superconducting fluctuations disappear rapidly (exponentially with reduced temperature) above a characteristic temperature T_0, as shown in figure 7(c). This rapid suppression of fluctuations was previously observed in $YBa_2Cu_3O_y$ [35, 36] and LSCO thin films [33] and associated to the presence of an energy cutoff [37–39] whose value is found to be doping-dependent [40]. The existence of this scale has been emphasized recently in various cuprates [41].

At low temperatures and low/intermediate fields, the superconductivity-related resistance is expected to display a linear behavior in temperature as follows from two-dimensional Aslamazov–Larkin fluctuations [31–34] at temperatures close to T_c. We adopt a simple phenomenological form which interpolates between the exponential behavior at high temperature and the Aslamazov–larkin behavior,

$$R^{\mathrm{AL}}_{\square,\mathrm{SC}}(H,T) = \frac{\mathrm{e}^{T/T_0} - \mathrm{e}^{T_c^{\mathrm{B}}/T_0}}{\sigma_{\square,0}}\theta(T - T_c^{\mathrm{B}}). \tag{6}$$

Indeed this expression behaves as $\propto T - T_c^{\mathrm{B}}$ at low temperature, where T_c^{B} will be termed the 'bulk' critical temperature. The parameters T_0, T_c^{B} and $\sigma_{\square,0}$ are taken to be functions of H alone, so all the temperature dependence is shown explicitly in equation (6).

Once $R_{\square,\mathrm{CO}}(T)$ was fixed, fits were done for the full set of data in the (H, T) plane, simultaneously minimizing the total square error respect to the parameters defining $R^{\mathrm{AL}}_{\square,\mathrm{SC}}(H,T)$. We took the parameters in the fit namely T_c^{B} and T_0 to be polynomials in H of degree 3.

For $\sigma_{\square,0}(H)$ we used a Lorentzian in H centered at $H = 0$. Because scans were done in field at fixed temperatures, the data used has very high resolution in field (nearly 1300 field values, with $\mu_0 H$ between 0 and 50 T) and much lower resolution in temperature (16 temperatures with higher resolution at low temperatures).

Constant field cuts of the resulting fit are shown with dashed lines in figure 7(b). It represents very well the experimental data except for the low temperature region ($\lesssim 8$ K) at intermediate fields. The root of the

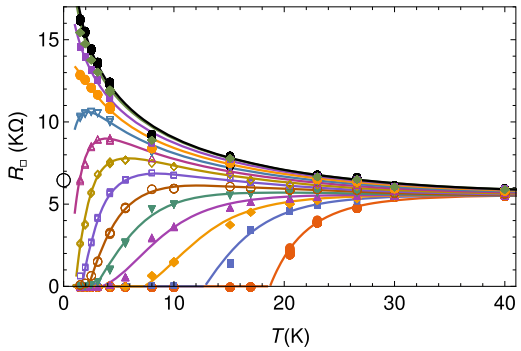

Figure 8. Temperature dependent resistance per square for sample 009 (LSCO/LSAO, $x = 0.09$) for different fields. Fields start from $\mu_0 H = 0$ T in the lower curve up to 48 T in intervals of 4 T. The black curve is the fit of the data without superconducting component at 54 T (black dots). The open black circle at $T = 0$ indicates the quantum of resistance $R_Q = h/(2e)^2$.

problem becomes clear upon inspection of panel (a). Notice that fluctuating superconductivity produce a visible magnetoresistance below the zero field from $T_{ONS} \approx 55$ K all the way down to T_c. Thus, the Aslamazov–Larkin regime is associated with a very broad regime of fluctuations characteristic of a two-dimensional superconductor. In contrast, as it is clear from figure 7(b), a much more rapid variation sets in below 8 K where points at intermediate fields are not fitted by the dashed lines (equation (6)). In other words, it is not possible to fit with a single Aslamazov–Larkin form both the broad fluctuating regime starting at T_{ONS} and the low-T regime at intermediate fields. This calls for a different mechanism setting in at low T, which we attribute to filamentary superconductivity short circuiting an otherwise finite low-T resistivity. In order to describe this effect we simply add an hyperbolic tangent cutoff to the superconducting component,

$$R_{\square,SC}(H,T) = R^{AL}_{\square,SC}(H,T)\tanh\left(\frac{T-T_c^F}{T_1}\right)\theta(T-T_c^F). \tag{7}$$

The theta function in equations (6) and (7) ensures that zero resistivity occurs at the maximum among the 'bulk' and the filamentary critical temperature parameters, T_c^B and T_c^F, respectively. For $T_c^F(H)$ and $T_1(H)$ we used a linear and quadratic function of H. Using equation (7) we obtain the full line fits of figure 7, which now work over the whole temperature range. We remark again that the fits are based on phenomenological functions and are not pretended to be derived from the theory of previous section. On the other hand they enable an accurate global representation of the data, which gives access to unbiased characteristic temperatures as a function of external parameters, as it will be shown next. On passing, we notice that signatures and extension of superconducting fluctuations in Nernst effect measurements were discussed in references [42, 43].

In order to further check the experimental result we have repeated the analysis on a different LSCO thin film with slightly different Sr content $x = 0.09$ but different growing conditions (figures 6(b) and 8). The occurrence of filamentary superconductivity is quite apparent from the low temperature drop in resistance in the curves showing semiconducting behavior. Notice again that this effect sets a characteristic temperature much lower than the onset of 'bulk' magnetoresistance effects $T_{ONS} \approx 40$ K. Thus, also this sample shows two well separated temperature scales for precursor superconducting effects which we associate with precursor 'bulk' superconductivity and precursor filamentary superconductivity.

Once the optimum surface is obtained in the (H, T) plane, it is possible to perform equal-resistivity plots as shown in figure 9. Here, we also show the maximum between $T_c^B(H)$ and $T_c^F(H)$ (red dashed line) which determines the upper boundary of the $R_\square(H,T) = 0$ region (colored blue). As expected $T_c^B(H)$ [$T_c^F(H)$] is dominant at low [high] field with a noticeable kink at the intersection. In order to extract the characteristic crossover temperatures defined in figure 5(c), we now determine the temperatures of the resistivity maximum $T_{max}(H)$ and minimum $T_{min}(H)$ by solving $\partial R_\square(H,T)/\partial T = 0$. Furthermore, we find the temperature $T_{inf}(H)$ of the resistivity inflection point, $\partial^2 R_\square(H,T)/\partial T^2 = 0$.

We first discuss the inflection point at low fields (blue dashed line). At high temperature, the resistivity has a positive curvature (figure 7(a)) which at small field is compensated by the onset of superconducting correlations. Therefore the inflection point is taken as the characteristic onset temperature, $T_{inf} \approx T_{ONS}$ for two-dimensional superconducting correlations (blue dashed line in figure 9). Notice that zero resistance shown by the blue region in figure 9 occurs at a much lower temperature (red dashed line), corresponding to three-dimensional phase coherence. This issue is discussed below.

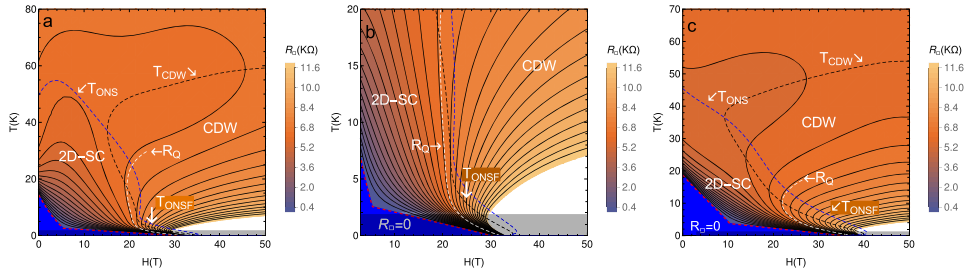

Figure 9. Phase diagram from experimental resistivity encoded on a color scale for: (a) and (b) sample 008 LSCO/STO, $x = 0.08$; c) sample 009 LSCO/LSAO, $x = 0.09$. The red dashed line is the extrapolated T_c below which $R_\square = 0$ (blue region). The black dashed line represents the zeroes of the first temperature derivative of the square resistance with the upper (lower) branch representing a minimum (maximum). The blue dashed line represents the zeroes of the second derivative, i.e., the inflection point which lays between the minimum and the maximum of each $R_\square(T)$ curve when they exists. Full lines are equal resistivity levels in intervals of 0.4 kΩ with the lower visible level close to T_c corresponding to 0.4 kΩ. The white dashed line is the isoline corresponding to the quantum of resistance. False colors encode the square resistance. The grey rectangle at the bottom indicates the extrapolated region (i.e. out of the range of available experimental data). Notice, however, that the leading behavior defining the foot is already quite clear from the available data in figure 7. (b) is a zoom of the critical region of (a).

Coming back to T_{ONS}, we see that it gets rapidly suppressed as a function of field and points to a clean quantum-critical point around $\mu_0 H_{CQCP} = 22\ T$ for sample 008 ($x = 0.08$). See figures 9(a) and (b). The existence of this clean quantum-critical point (and an associated plateau) was already proposed, together with the existence of a two-stage transition in reference [44]. A two-stage transition was subsequently reported and discussed in reference [45]. As also observed in reference [44], the resistivity per square at this plateau corresponds quite closely to the quantum of resistance R_Q indicated by an open circle at the origin in figures 7(a) and (b). $R_\square = R_Q$ is also indicated with a white dashed line in figure 9. Theory predicts that in the case of a perfectly self-dual insulator-superconductor transition, the critical resistance should be equal to the quantum of resistance [12, 46, 47]. Real systems may show deviation from perfect duality and a different critical resistance. Interestingly enough, the present way of plotting data reveals that R_Q indeed coincides with the separatrix line over a broad temperature and field range. A study in which the carrier density in a single layer of the same material was tuned with an electric field [48] found $R_\square = R_Q$ at the insulator-superconductor transition, in good agreement with the critical resistance in the present study. It is worth mentioning that in the latter experiment the lowest temperature measured was 4.3 K, so the filamentary superconductivity observed here was not accessible (cf figure 9(b)).

At high fields and below $T \approx 60$ K, the polycrystalline CDW phase becomes relevant. The crossover is characterized by a change from metallic behavior at high temperature to semiconducting behavior at low temperature, justifying the choice $T_{min} \approx T_{CDW}$ as the characteristic CDW onset temperature (black dashed line). We see that T_{CDW} approximately mirrors the behavior of T_{ONS} and drops dramatically with decreasing field in the critical region.

At low temperatures and intermediate fields a maximum of the resistivity appears preceded by a nearby inflection point (see for example the blue curve at intermediate field in figures 7(a) and(b)) and figure 8. We associate this behavior with the onset of filamentary superconducting transition T_{ONSF}. Indeed, T_{ONSF} as function of H shows the expected characteristic 'foot' in the phase diagram of figure 9 (see figures 4(a) and 5(b)). Another fingerprint of filamentary superconductivity is that both T_{inf} (dashed blue line) and T_{max} (dashed black line) are very close in this region (cf figure 5(c)).

Figure 9(c) shows the phase diagram for sample 009 with $x = 0.09$. In this case the drop of T_{ONS} is more gradual, which could be related to a more gradual decrease of the stiffness when disorder is increased (compare T_{ONS}, T_{ONSF} with the light blue curve in figure 4). In any case, since samples 008 and 009 are grown under different conditions and on different substrates, the fact that filamentary superconductivity is observed in both cases pleads for the universality of the phase diagram in this region of doping. Interestingly an analysis in a wider doping range with a different fitting methodology reaches similar conclusions [5].

4. Discussion

In this work, we have taken a simplified model for CDW-superconductivity competition. For the CDW our model has only two possible 'colors', A/B. Colors correspond to different realizations of a broken symmetry phase that are equivalent by an operation of the high (unbroken) symmetry group.

We expect that increasing the number of CDW colors does not change substantially our theoretical results. Also in our modeling we do not need to specify the microscopic origin of CDW colors. There are presently several possibilities in the case of cuprates which we now discuss: (i) Scanning tunneling microscopy [49] have shown that underdoped cuprates are characterized by CDW domains with 4-lattice spacing periodicity separated by discommensurations. The translation operation naturally defines 4 colors for the CDW for a given orientation of the unidirectional CDW (see figure 3F in reference [49]). (ii) A related possibility is that stripes are formed at high temperatures but are metallic and half-filled [50] and develop a secondary CDW Peierls stability along the stripe which, in strong coupling, can be seen as a lattice of Cooper pairs [51]. It is natural to describe this state with an effective negative-U Hubbard model along the chains, with an associate quasidegenerate superconducting state. (iii) Yet another possibility is suggested by a microscopic analysis which finds an incommensurate CDW in oxygen with d-wave symmetry which can be rotated to d-wave superconductivity [52, 53]. Here, an Ising order parameter controls excess charge in x-oriented Cu–O–Cu bonds with respect to y-oriented Cu–O–Cu bonds, which can be associated to the two possible colors of our description. (iv) Alternatively, one can see the incommensurate nature in (iii) as consequence of the weak-coupling analysis and consider a locally commensurate (strong coupling) version of the theory with superconductivity nucleating at the discommensurations, as in (i). More experimental and theoretical work is needed to establish which scenario occurs in a particular material.

The disorder-induced coexistence of superconductivity and CDW can be seen as a form of intertwined order in the sense of reference [8]. However, these authors treat pair-density-wave order (a self-organized version of the Fulde–Ferell–Larkin–Ovchinikov state [54, 55]) as the primary order and CDW as a parasitic order. In the present scenario, both CDW and bulk superconducting order are primary, while filamentary superconductivity is parasitic.

We have used transport data to derive a phase diagram assuming the magnetic field as tuning parameter (figure 9). We expect similar phase diagrams using lattice strain [23], field effect [48], or simply doping as tuning parameters. Indeed, comparing figures 9(a) and (c), one concludes that doping plays a role similar to that of magnetic field, since the phase diagram appears rigidly shifted [5]. The advantage of the magnetic field is that, being associated with a small energy scale, a high resolution scan of the crossovers is possible.

The main difference between the theoretical and the experimental phase diagram discussed is that superconductivity in the former is replaced by two-dimensional fluctuating superconductivity in the latter. One should take into account that the theory does not include long-range interactions and quantum fluctuations which are expected to suppress the zero resistance state [56]. Therefore, we associate T_{ONS} to the transition temperature of the model without these effects. With this caveat, the two phase diagrams are in excellent agreement, in particular, the experimental phase diagram clearly exhibits the foot-like behavior indicating filamentary superconductivity.

After the theory part of this work was completed and posted in reference [4], reference [57] appeared, where a very similar phase diagram was derived in a model of superconductivity competing with incommensurate CDW (rather than commensurate as here) in the presence of disorder. The kind of topological defects considered are different—the latter model does not predict filamentary superconductivity. Nevertheless, the fact that the essential physical outcomes of the two approaches are similar pleads in favour of a rather generic character of disorder-induced superconductvity inside an otherwise stable CDW phase.

The effect of the competition between CDWs and superconductivity in the presence of disorder, with the magnetic field acting as a driving parameter was also investigated in reference [58], within a nonlinear sigma model, and the theory was used to discuss three-dimensional CDW order in $YBa_2Cu_3O_y$, under magnetic field. The possibility of residual local superconducting order was discussed thereby, but the occurrence of topologically protected re-entrant filamentary superconductivity was not investigated. From the experimental point of view, the competition and/or coexistence between superconductivity and stripe [59, 60] or CDW [60–63] order, possibly within an inhomogeneous scenario, have been repeatedly assessed and discussed in cuprates.

It has been proposed that in some underdoped cuprates long-range superconducting order [64–66] is frustrated by a peculiar symmetry of the superconducting state. It is not clear at the moment if this effect contributes also to the difference between T_{ONS} and T_c in the present samples. One can reverse the argument and argue that filamentary superconductivity is particularly unsuited for three-dimensional phase locking, as the filaments in one plane will in general not coincide with the filaments in the next plane, thus frustrating Josephson coupling. Whether this is the underlying reason for the lack of three-dimensional phase locking in experiments deserves further scrutiny.

The deduced phase diagram is not peculiar of the sample analyzed in figure 9. Remarkably, an almost identical phase diagram has been derived by completely different techniques in a different material, namely specific heat measurements [67] in $YBa_2Cu_3O_y$, suggesting that this phase diagram is a quite generic feature

of underdoped cuprates. It is suggestive that the experimental stiffness as a function of temperature also has the tendency to develop a foot above standard theoretical predictions (see for example, figure 4 of reference [68]).

The model presented here is very general and applies to other systems as well, where the balance between CDW and superconductivity can produce a topologically protected intertwined order. A particularly interesting model system is the Cu-intercalated dichalcogenide 1T–$TiSe_2$. In this system, scanning tunneling microscopy [69] shows a commensurate CDW in the undoped system with domain walls appearing upon Cu intercalation. Simultaneously with the latter, superconductivity appears too. The link between CDW discomensurations and superconductivity emerges also from magnetoresistance experiments in gated two-dimensional materials [70, 71] and from x-ray experiments under pressure [72]. A McMillan–Ginzburg–Landau model specific for 1T–$TiSe_2$ shows indeed that superconductivity nucleates at discommensurations of the CDW in agreement with our approach [73]. Filamentary superconductivity has also been inferred by phenomenological analyses of transport in $LaAlO_3/SrTiO_3$ heterostructures [74], in ZrNCl and other dichalcogenides [75].

In summary, we propose that in systems in which attractive interactions drive CDW and superconductivity with similar energies disorder may break the CDW into domains with filamentary superconductivity emerging at the interfaces. Long-range superconductivity eventually takes place when the temperature is low enough to allow the phase locking between the superconducting regions.

This adds to the case of ^{4}He and suggest that the phenomenon at hand is very general. In solids, remarkably, melting occurs first at the surface [76]. Thus, when a polycrystal is driven just below the melting temperature, the less stable liquid phase nucleates at the interface, which represents a classical analog of the above studied phenomena and underpins again its generality.

Acknowledgments

JL is very much indebted with Andrea Cavagna and Carlo Di Castro for important discussions at the early stages of this work. JL and SC thank all the colleagues of the ESPCI in Paris for their warm hospitality and for many useful discussion while this work was done. The work at the KU Leuven has been supported by the FWO Programmes and Methusalem Funding by the Flemish Government. Research at IIT Kanpur has been supported by the JC Bose National Fellowship (RCB). Part of this work has been founded by EuroMagNET II under the EU contract number 228043. SC and MG acknowledge financial support of the University of Rome Sapienza, under the Ateneo 2017 (prot. RM11715C642E8370), Ateneo 2018 (prot. RM11816431DBA5AF), and Ateneo 2019 (prot. RM11916B56802AFE) projects. JL acknowledges financial support from Italian MAECI through collaborative project SUPERTOP-PGR04879 and bilateral project AR17MO7 and from Regione Lazio (L.R. 13/08) under project SIMAP. Part of the work was supported through the Chaire Joliot at ESPCI Paris. This work was also supported by EU through the COST action CA16218 and from Italian MIUR through Project No. PRIN 2017Z8TS5B.

ORCID iDs

Brigitte Leridon https://orcid.org/0000-0002-0996-352X
Sergio Caprara https://orcid.org/0000-0001-8041-3232
Baptiste Vignolle https://orcid.org/0000-0001-8775-1701
Alessandro Attanasi https://orcid.org/0000-0002-6280-5862
Marco Grilli https://orcid.org/0000-0001-5607-7996
José Lorenzana https://orcid.org/0000-0001-7426-2570

References

[1] Nozières P and Schmitt-Rink S 1985 Bose condensation in an attractive fermion gas: from weak to strong coupling superconductivity *J. Low Temp. Phys.* **59** 195–211
[2] London F 1954 *Superfluids: Macroscopic Theory of Superfluid Helium* (New York: Dover)
[3] Balibar S and Caupin F 2008 Supersolidity and disorder *J. Phys.: Condens. Matter* **20** 173201
[4] Attanasi A 2008 Competition between superconductivity and charge density waves: the role of disorder *PhD Thesis* (Sapienza Università di Roma) arXiv:0906.1159
[5] Caprara S, Grilli M, Lorenzana J and Leridon B 2020 Doping-dependent competition between superconductivity and polycrystalline charge density waves *SciPost Phys.* **8** 003
[6] Gerber S *et al* 2015 Three-dimensional charge density wave order in $YBa_2Cu_3O_{6.67}$ at high magnetic fields *Science* **350** 949–52

[7] Phillips J C 1991 Electronic disorder, gap states, orbital depairing, and dynamics of percolative superconductors near T_c *Phys. Rev.* B **43** 11415
[8] Fradkin E, Kivelson S A and Tranquada J M 2015 Colloquium: theory of intertwined orders in high temperature superconductors *Rev. Mod. Phys.* **87** 457–82
[9] Micnas R, Ranninger J and Robaszkiewicz S 1990 Superconductivity in narrow-band systems with local nonretarded attractive interactions *Rev. Mod. Phys.* **62** 113–71
[10] Anderson P W 1958 Random-phase approximation in the theory of superconductivity *Phys. Rev.* **112** 1900–16
[11] Liu K-S and Fisher M E 1972 Quantum lattice gas and the existence of a supersolid *J. Low Temp. Phys.* **10** 655
[12] Cha M C, Fisher M P, Girvin S M, Wallin M and Young A P 1991 Universal conductivity of two-dimensional films at the superconductor-insulator transition *Phys. Rev.* B **44** 6883–902
[13] Binder K 1983 Random-field induced interface widths in Ising systems *Z. Phys. B: Condens. Matter* **50** 343–52
[14] Imry Y and Ma S-k 1975 Random-field instability of the ordered state of continuous symmetry *Phys. Rev. Lett.* **35** 1399–401
[15] Kirkpatrick S 1973 Percolation and conduction *Rev. Mod. Phys.* **45** 574–88
[16] Cuccoli A, Roscilde T, Tognetti V, Vaia R and Verrucchi P 2003 Quantum Monte Carlo study of S = 1/2 weakly anisotropic antiferromagnets on the square lattice *Phys. Rev.* B **67** 104414
[17] Kosterlitz J M and Thouless D J 1973 Metastability and phase transitions in two dimensional systems *J. Phys.* C **6** 1181
[18] Miao H *et al* 2017 High-temperature charge density wave correlations in $La_{1.875}Ba_{0.125}CuO_4$ without spin-charge locking *Proc. Natl. Acad. Sci.* **114** 12430–5
[19] Nie L, Tarjus G and Kivelson S A 2014 Quenched disorder and vestigial nematicity in the pseudogap regime of the cuprates *Proc. Natl. Acad. Sci.* **111** 7980–5
[20] Capati M *et al* 2015 Electronic polymers and soft-matter-like broken symmetries in underdoped cuprates *Nat. Commun.* **6** 10
[21] Ando Y, Komiya S, Segawa K, Ono S and Kurita Y 2004 Electronic phase diagram of high-T_c cuprate superconductors from a mapping of the in-plane resistivity curvature *Phys. Rev. Lett.* **93** 267001
[22] Pelc D, Popčević P, Požek M, Greven M and Barišić N 2019 Unusual behavior of cuprates explained by heterogeneous charge localization *Sci. Adv.* **5** eaau4538
[23] Kim H-H *et al* 2018 Uniaxial pressure control of competing orders in a high-temperature superconductor *Science* **362** 1040–4
[24] Kivelson S A *et al* 2003 How to detect fluctuating stripes in the high-temperature superconductors *Rev. Mod. Phys.* **75** 1201–41
[25] Wu T *et al* 2011 Magnetic-field-induced charge-stripe order in the high-temperature superconductor YBa2Cu3O y *Nature* **477** 191–4
[26] Campi G *et al* 2015 Inhomogeneity of charge-density-wave order and quenched disorder in a high-T_c superconductor *Nature* **525** 359
[27] Doiron-Leyraud N *et al* 2007 Quantum oscillations and the Fermi surface in an underdoped high-T_c superconductor *Nature* **447** 565
[28] Ramshaw B J *et al* 2015 Quasiparticle mass enhancement approaching optimal doping in a high-T_c superconductor *Science* **348** 317
[29] Badoux S *et al* 2016 Change of carrier density at the pseudogap critical point of a cuprate superconductor *Nature* **531** 210
[30] Chan M K *et al* 2016 Single reconstructed Fermi surface pocket in an underdoped single-layer cuprate superconductor *Nat. Commun.* **7** 12244
[31] Aslamazov L G and Larkin A I 1968 Effect of fluctuations on the properties of a superconductor above the critical temperature *Sov. Phys.-Solid State* **10** 875
[32] Aslamasov L G and Larkin A I 1968 The influence of fluctuation pairing of electrons on the conductivity of normal metal *Phys. Lett.* A **26** 238–9
[33] Leridon B, Vanacken J, Wambecq T and Moshchalkov V V 2007 Paraconductivity of underdoped $La_{2-x}Sr_xCuO_4$ thin-film superconductors using high magnetic fields *Phys. Rev.* B **76** 012503
[34] Caprara S, Grilli M, Leridon B and Vanacken J 2009 Paraconductivity in layered cuprates behaves as if due to pairing of nearly free quasiparticles *Phys. Rev.* B **79** 024506
[35] Leridon B, Defossez A, Dumont J, Lesueur J and Contour J P 2001 Conductivity of underdoped $YBa_2Cu_3O_{7-?}$: evidence for incoherent pair correlations in the pseudogap regime *Phys. Rev. Lett.* **87** 197007
[36] Leridon B, Defossez A, Dumont J, Lesueur J and Contour J P 2003 Leridon et al Reply: *Phys. Rev. Lett.* **90** 179704
[37] Vidal F *et al* 2002 On the consequences of the uncertainty principle on the superconducting fluctuations well inside the normal state *Europhys. Lett.* **59** 754–60
[38] Mishonov T M, Pachov G V, Genchev I N, Atanasova L A and Damianov D C 2003 Kinetics and Boltzmann kinetic equation for fluctuation Cooper pairs *Phys. Rev.* B **68** 545251–8
[39] Caprara S, Grilli M, Leridon B and Lesueur J 2005 Extended paraconductivity regime in underdoped cuprates *Phys. Rev.* B **72** 104509
[40] Luo C W *et al* 2003 Comment on conductivity of underdoped $YBa_2Cu_3O_{7-\delta}$: evidence for incoherent pair correlations in the Pseudogap regime *Phys. Rev. Lett.* **90** 179703
[41] Popčević P *et al* 2018 Percolative nature of the direct-current paraconductivity in cuprate superconductors *npj Quantum Mater.* **3** 42
[42] Chang J *et al* 2012 Decrease of upper critical field with underdoping in cuprate superconductors *Nat. Phys.* **8** 751–6
[43] Tafti F F *et al* 2014 Nernst effect in the electron doped cuprate superconductor $Pr_{2-x}Ce_xCuO_4$: superconducting fluctuations, upper critical field H_{c2}, and the origin of the T_c dome *Phys. Rev.* B **90** 024519
[44] Leridon B *et al* 2013 Double criticality in the magnetic field-driven transition of a high-T_c superconductor (arXiv:1306.4583)
[45] Shi X *et al* 2014 Two-stage magnetic-field-tuned superconductor-insulator transition in underdoped $La_{2-x}Sr_xCuO_4$ *Nat. Phys.* **10** 437–43
[46] Fisher M P A, Grinstein G and Girvin S M 1990 Presence of quantum diffusion in two dimensions: universal resistance at the superconductor/insulator transition *Phys. Rev. Lett.* **64** 587
[47] Fisher M P A 1990 Quantum phase transitions in disordered two-dimensional superconductors *Phys. Rev. Lett.* **65** 923
[48] Bollinger A T *et al* 2011 Superconductor-insulator transition in $La_{2-x}Sr_xCuO_4$ at the pair quantum resistance *Nature* **472** 458–60
[49] Mesaros A *et al* 2016 Commensurate 4a0-period charge density modulations throughout the Bi2Sr2CaCu2O8+x pseudogap regime *Proc. Natl. Acad. Sci.* **113** 12661–6
[50] Lorenzana J and Seibold G 2002 Metallic mean-field stripes, incommensurability, and chemical potential in cuprates *Phys. Rev. Lett.* **89** 136401

[51] Bosch M, van Saarloos W and Zaanen J 2001 Shifting Bragg peaks of cuprate stripes as possible indications for fractionally charged kinks *Phys. Rev.* B **63** 092501
[52] Sachdev S and La Placa R 2013 Bond order in two-dimensional metals with antiferromagnetic exchange interactions *Phys. Rev. Lett.* **111** 027202
[53] Efetov K B, Meier H and Pépin C 2013 Pseudogap state near a quantum critical point *Nat. Phys.* **9** 442–6
[54] Larkin A I and Ovchinnikov Y N 1964 Nonuniform state of superconductors *Zh. Eksperim. i Teor. Fiz.* **47** 1136
Larkin A I and Ovchinnikov Y N 1965 *Sov. Phys. JETP* **20** 762
[55] Fulde P and Ferrell R A 1964 Superconductivity in a strong spin-exchange field *Phys. Rev.* **135** A550–63
[56] Emery V J and Kivelson S A 1995 Dimensional crossover of charge-density wave correlations in the cuprates *Nature* **374** 434
[57] Yu Y and Kivelson S A 2019 Fragile superconductivity in the presence of weakly disordered charge density waves *Phys. Rev.* B **99** 144513
[58] Caplan Y and Orgad D 2017 Dimensional crossover of charge-density wave correlations in the cuprates *Phys. Rev.* B **119** 144513
[59] Lake B *et al* 2002 Antiferromagnetic order induced by an applied magnetic field in a high-temperature superconductor *Nature* **415** 299–302
[60] Wen J–J *et al* 2019 Observation of two types of charge-density-wave orders in superconducting $La_{2-x}Sr_xCuO_4$ *Nat. Commun.* **10** 3269
[61] Chang J *et al* 2012 Direct obervation of competition between superconductivity and charge density wave order in $YBa_2Cu_3O_{6.67}$ *Nat. Phys.* **8** 871–6
[62] LeBoeuf D *et al* 2013 Thermodynamic phase diagram of static charge order in underdoped $YBa_2Cu_3O_y$ *Nat. Phys.* **9** 79–83
[63] Arpaia R *et al* 2019 Dynamical charge density fluctuations pervading the phase diagram of a Cu-based high-T_c superconductor *Science* **365** 906–10
[64] Himeda A, Kato T and Ogata M 2002 Stripe states with spatially oscillating *d*-wave superconductivity in the two-dimensional *t*-*t*′-J model *Phys. Rev. Lett.* **88** 117001
[65] Li Q, Hücker M, Gu G D, Tsvelik A M and Tranquada J M 2007 Two-dimensional superconducting fluctuations in stripe-ordered $La_{1.875}Ba_{0.125}CuO_4$ *Phys. Rev. Lett.* **99** 067001
[66] Berg E *et al* 2007 Dynamical layer decoupling in a stripe-ordered high-T_c superconductor *Phys. Rev. Lett.* **99** 127003
[67] Kačmarčík J *et al* 2018 Unusual interplay between superconductivity and field-induced charge order in YBa_2Cu_3 Oy *Phys. Rev. Lett.* **121** 167002
[68] Baity P G *et al* 2016 Effective two-dimensional thickness for the Berezinskii–Kosterlitz–Thouless-like transition in a highly underdoped $La_{2-x}Sr_xCuO_4$ *Phys. Rev.* B **93** 024519
[69] Yan S *et al* 2017 Influence of domain walls in the incommensurate charge density wave state of Cu intercalated 1T–$TiSe_2$ *Phys. Rev. Lett.* **118** 106405
[70] Li L J *et al* 2016 Controlling many-body states by the electric-field effect in a two-dimensional material *Nature* **529** 185–9
[71] Li L *et al* 2019 Anomalous quantum metal in a 2D crystalline superconductor with intrinsic electronic non-uniformity *Nano Lett.* **19** 4126–33
[72] Joe Y I *et al* 2014 Emergence of charge density wave domain walls above the superconducting dome in 1T–$TiSe_2$ *Nat. Phys.* **10** 421–5
[73] Chen C *et al* 2019 Discommensuration-driven superconductivity in the charge density wave phases of transition-metal dichalcogenides *Phys. Rev.* B **99** 121108
[74] Caprara S *et al* 2013 Multiband superconductivity and nanoscale inhomogeneity at oxide interfaces *Phys. Rev.* B **88** 020504(R)
[75] Dezi G, Scopigno N, Caprara S and Grilli M 2018 Negative electronic compressibility and nanoscale inhomogeneity in ionic-liquid gated two-dimensional superconductors *Phys. Rev.* B **98** 214507
[76] Frenken J W M and Van Der Veen J F 1985 Observation of surface melting *Phys. Rev. Lett.* **54** 134–7